

Probabilistic mapping of deep brain stimulation effects in essential tremor



Till A Dembek^{a,d,*}, Michael T Barbe^a, Mattias Åström^{b,c}, Mauritius Hoevens^d, Veerle Visser-Vandewalle^d, Gereon R Fink^a, Lars Timmermann^a

^aDepartment of Neurology, University of Cologne, Cologne, Germany

^bDepartment of Biomedical Engineering, Linköping University, Linköping, Sweden

^cMedtronic Neuromodulation, Medtronic Eindhoven Design Center, Eindhoven, The Netherlands

^dDepartment of Stereotaxy and Functional Neurosurgery, University of Cologne, Cologne, Germany

ARTICLE INFO

Article history:

Received 21 July 2016

Received in revised form 6 October 2016

Accepted 16 November 2016

Available online 17 November 2016

Keywords:

Deep brain stimulation

Essential tremor

Probabilistic mapping

Zona incerta

ABSTRACT

Objective: To create probabilistic stimulation maps (PSMs) of deep brain stimulation (DBS) effects on tremor suppression and stimulation-induced side-effects in patients with essential tremor (ET).

Method: Monopolar reviews from 16 ET-patients which consisted of over 600 stimulation settings were used to create PSMs. A spherical model of the volume of neural activation was used to estimate the spatial extent of DBS for each setting. All data was pooled and voxel-wise statistical analysis as well as nonparametric permutation testing was used to confirm the validity of the PSMs.

Results: PSMs showed tremor suppression to be more pronounced by stimulation in the zona incerta (ZI) than in the ventral intermediate nucleus (VIM). Paresthesias and dizziness were most commonly associated with stimulation in the ZI and surrounding thalamic nuclei.

Discussion: Our results support the assumption, that the ZI might be a very effective target for tremor suppression. However stimulation inside the ZI and in its close vicinity was also related to the occurrence of stimulation-induced side-effects, so it remains unclear whether the VIM or the ZI is the overall better target. The study demonstrates the use of PSMs for target selection and evaluation. While their accuracy has to be carefully discussed, they can improve the understanding of DBS effects and can be of use for other DBS targets in the therapy of neurological or psychiatric disorders as well. Furthermore they provide a priori information about expected DBS effects in a certain region and might be helpful to clinicians in programming DBS devices in the future.

© 2016 The Authors. Published by Elsevier Inc. This is an open access article under the CC BY-NC-ND license (<http://creativecommons.org/licenses/by-nc-nd/4.0/>).

1. Introduction

Essential tremor (ET) is the most common adult movement disorder, affecting around 0.9% of the population worldwide (Louis and Ferreira, 2010). Medical treatment fails in up to 55% of the patients (Flora et al., 2010). For those patients Deep Brain Stimulation (DBS) of the ventral intermediate nucleus (VIM) of the thalamus has become a well-accepted treatment option with long-term improvement of tremor scores between 50 and 80% (Koller et al., 2001; Pahwa et al., 2006; Zhang et al., 2010). Despite these results, open questions remain regarding the optimal neuroanatomical target for DBS in ET. Recent studies suggest that stimulation of more ventral structures like the zona incerta

(ZI), which is part of the posterior subthalamic area (PSA), is equally or even more effective in suppressing tremor than VIM stimulation (Barbe et al., 2011; Blomstedt et al., 2010; Sandvik et al., 2012; Xie et al., 2012). Additionally, stimulation-induced side-effects, such as paresthesia, disequilibrium/gait-ataxia, and dysarthria (Fasano et al., 2010; Flora et al., 2010; Mücke et al., 2014), are increasingly spotlighted since they interfere with selecting the optimal stimulation parameters for tremor suppression (Barbe et al., 2014). In ET, only few studies analyzed clinical outcome of DBS with regard to electrode location (Barbe et al., 2011; Phibbs et al., 2014; Sandvik et al., 2012) and only one study specifically investigated the origin of stimulation-induced side-effects (Fytagoridis et al., 2013). These studies, however, did not account for the spatial distribution of stimulation, the so-called ‘volume of tissue activated’ or ‘volume of neural activation’ (VNA). Since spread of electrical stimulation into certain neuroanatomical structures is one of the crucial factors for both beneficial and adverse DBS effects, analysis of DBS effects based on VNAs rather than mere electrode locations seems mandatory. Several approaches for estimating the VNA have been put forward, some relying on clinical data (Kuncel et al., 2008; Mädler and Coenen, 2012)

Abbreviations: DBS, Deep brain stimulation; ET, Essential tremor; PSA, Posterior subthalamic area; PSM, Probabilistic stimulation map; VIM, Ventral intermediate nucleus; VNA, Volume of neural activation; ZI, Zona incerta.

* Corresponding author at: Department of Neurology, University of Cologne, Kerpener Strasse 62, D-50937 Cologne, Germany.

E-mail address: till.dembek@uk-koeln.de (T.A. Dembek).

and some relying on biophysically based computer simulations (Astrom et al., 2015; McIntyre et al., 2004) or on training artificial neural networks (Chaturvedi et al., 2013). In DBS for Parkinson's disease, there have been approaches to use VNAs on a patient level to analyze the neuroanatomical origins of DBS effects (Astrom et al., 2010; Frankemolle et al., 2010; Maks et al., 2009; Mikos et al., 2011). On a cohort level, different groups created so called probabilistic stimulation maps (PSMs), where clinical stimulation data is pooled over a patient collective and mapped into neuroanatomical space (Butson et al., 2011; Cheung et al., 2014; Eisenstein et al., 2014; Phibbs et al., 2014). While different methods of creating PSMs exist, only Eisenstein et al. addressed the issue of statistically validating their PSMs (Eisenstein et al., 2014). The aim of our study was to create statistically validated PSMs for DBS-induced tremor suppression and side-effect occurrence in ET-patients. We hypothesized that the created PSMs would show distinct spatial distributions for tremor suppression and the occurrence of side-effects. We also hypothesized that stimulation of the ZI might be more effective in suppressing tremor than stimulation of the VIM proper.

2. Materials and methods

2.1. Patients and clinical data

We analyzed retrospective data of 16 ET-patients with bilateral VIM-DBS, who were part of a previously published study (Barbe et al., 2011). Surgical practice in our center resulted in some of the ventral electrodes being placed ventral of the VIM in the PSA/ZI. During the aforementioned study, the patients underwent a well-documented and thorough monopolar review by an experienced movement disorders specialist (MTB). Stimulation was assessed at each electrode separately, beginning at the most ventral electrode, with steps in stimulation amplitude of 1 V up to 6 V. Pulse width was set to 60 μ s and stimulation frequency to 130 Hz. Electrode impedances were ensured to be below 2000 Ohms. Occurrence of side-effects, including paresthesia, dysarthria, dizziness and disturbed vision, was recorded. Furthermore, an unblinded rating of tremor suppression relative to the stimulation OFF (in percent) was provided for contralateral upper limb postural and intention tremor. In total, 606 different stimulation configurations were tested. Since not all patients showed both postural and intention tremor in both upper limbs, 568 ratings for postural and 358 ratings for intention tremor were available.

2.2. Electrode localization

Primary targeting was performed using the stereotactic planning system STP 3.50 (Stryker/Leibinger, Freiburg, Germany) and was based on fused preoperative CT and MRI scans. Lead positioning was optimized using intraoperative electrophysiological recordings and test stimulation. Final electrode positions were identified by stereotactic x-ray scans, taken after both leads had been fixed. Stereotactic x-ray consisted of two orthogonal images in the frontal and lateral orientation taken with fiducial markers mounted onto the stereotactic frame. Marker locations in both projections determined the x-ray focus and image plane, which allowed calculating three-dimensional stereotactic coordinates of each electrode using an in-house software module (STVX 3), which implements the well-established algorithm of Siddon and Barth (1987). Coordinates were handed over to the planning system and projected onto the preoperative MRI. Electrode positions, the position of the posterior commissure (PC), and the center of the optic chiasm (OX) were determined in relation to the anterior commissure (AC) and then transformed into the atlas space by using a previously published fiducial based method (Videen et al., 2008). Finally all electrode locations were transformed to lie inside the left hemisphere, to allow for their contribution to a single PSM (Fig. 1).

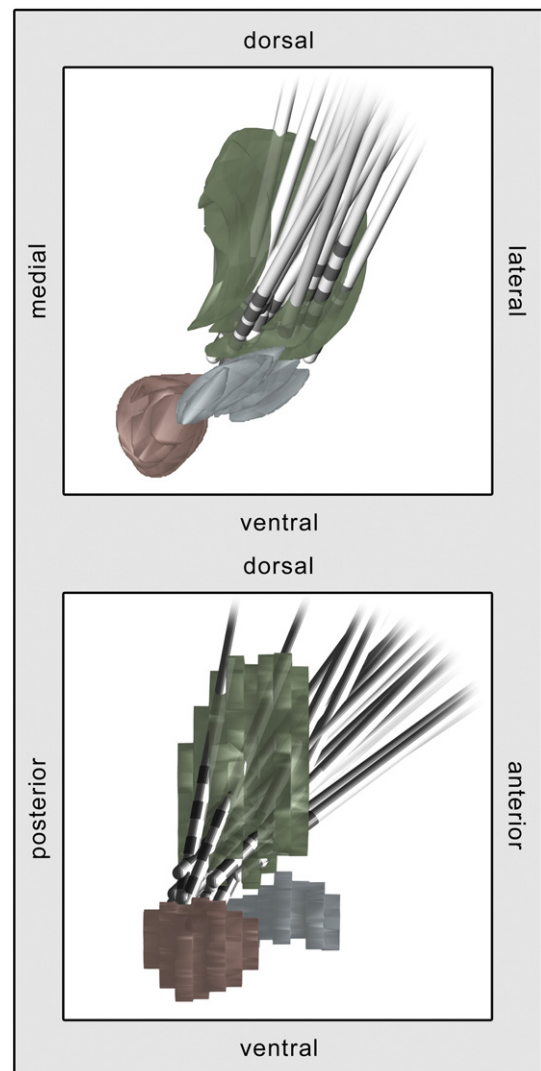


Fig. 1. Electrode locations. All examined electrodes are displayed together with neuroanatomical structures. Electrode coordinates were transformed into standardized atlas space. Right-hemispheric electrodes were mirrored to the left hemisphere. Neuroanatomical structures shown are the ventral intermediate nucleus (VIM, green), the subthalamic nucleus (blue), and the red nucleus (red). All structures were derived from the 'Atlas of the Human Brain' by Mai et al. (2008).

2.3. Neuroanatomical atlas

A 3-dimensional version of the 'Atlas of the Human Brain, 3rd edition' by Mai et al. (2008), which features coronal slices with 1.3 mm spacing in the thalamic region, was used as anatomical reference. Relevant brain structures were extracted from the two-dimensional atlas slices and converted to three-dimensional, voxel-based stacks. Spatial resolution was set to 0.5 mm in all three dimensions, while spatial accuracy along the y-axis remained at 1.3 mm.

2.4. Volume of neural activation

To estimate the extent of DBS, several VNA-models have been put forward. Regardless of their complexity most published models suggest a more or less spherical VNA for stimulation via standard ring electrodes and under the assumption of isotropic tissue (Astrom et al., 2015; Chaturvedi et al., 2013; McIntyre et al., 2004). For this paper, we thus used a computationally simple, spherical VNA-estimate which we based on clinical data for 90 μ s thalamic stimulation by Kuncel et al.

(2008). To be able to calculate radius estimates for other pulse widths as well, we also incorporated the work of Astrom et al. (2015). The VNA-radius r was calculated using the stimulation current amplitude I and the pulse width pw according to the following equation (see Appendix 1 for its derivation and validation):

$$r = \left(\frac{pw}{90 \mu s} \right)^{0.3} * \sqrt{0.72 \frac{Vm}{A} * \frac{I}{165 V/m}} \quad (1)$$

Impedances of 1000 Ohms were assumed for the generation of the VNAs.

2.5. Probabilistic stimulation maps

For each patient and stimulation setting a voxel-based VNA-estimate was created, centered on the coordinates of the respective electrode. Each voxel of the VNA-estimate was then assigned the corresponding clinical scores for each symptom. For side-effects these were binary values with ones reflecting the occurrence of a side-effect and zeros reflecting its absence during stimulation. For tremor suppression these were values ranging from 0% to 100% indicating tremor suppression relative to baseline. Because tremor suppression was significantly correlated with stimulation amplitude (postural tremor: Spearman's rho $\rho = 0.512$, $p < 0.01$; intention tremor: Spearman's rho $\rho = 0.344$, $p < 0.01$) and since the goal in clinical programming is to achieve maximum tremor suppression with as little stimulation as possible, tremor suppression scores were divided by the stimulation amplitude, before

assigning them to their respective voxels. All VNAs for a symptom were then pooled into atlas space. Mean clinical scores were then calculated for every voxel to create a 'mean effect image' (Eisenstein et al., 2014). Also the number of clinical scores for each voxel was counted to create an 'n-image'. All voxels, which did not receive clinical scores from at least $n = 15$ VNAs, were discarded to ensure the validity of voxel-wise statistical testing (Fig. 2).

2.6. Voxel-wise statistical analysis

Voxel-wise statistical tests were performed for each remaining voxel. Due to the nature of our data, we used one-sided Wilcoxon signed-rank tests for tremor suppression scores and binomial tests for side-effects. Null-hypotheses for statistical testing were that stimulation of a voxel led to no tremor suppression or side-effect occurrence. p-Values for each examined voxel were stored inside the 'p-image'. Finally, we created 'significant mean effect images', by discarding all voxels from the 'mean effect image', which did not show significant results ($p < 0.05$) in the 'p-image' (Fig. 2).

2.7. Type 1 error correction for multiple comparisons

As proposed by Eisenstein et al., we used a nonparametric permutation algorithm to address the problem of multiple comparisons that is inherent to voxel-wise statistical analysis (Eisenstein et al., 2014). The permutation algorithm allows comparing the overall statistical significance of a real p-image to the overall significances of p-images derived from permuted datasets. As marker for the overall statistical

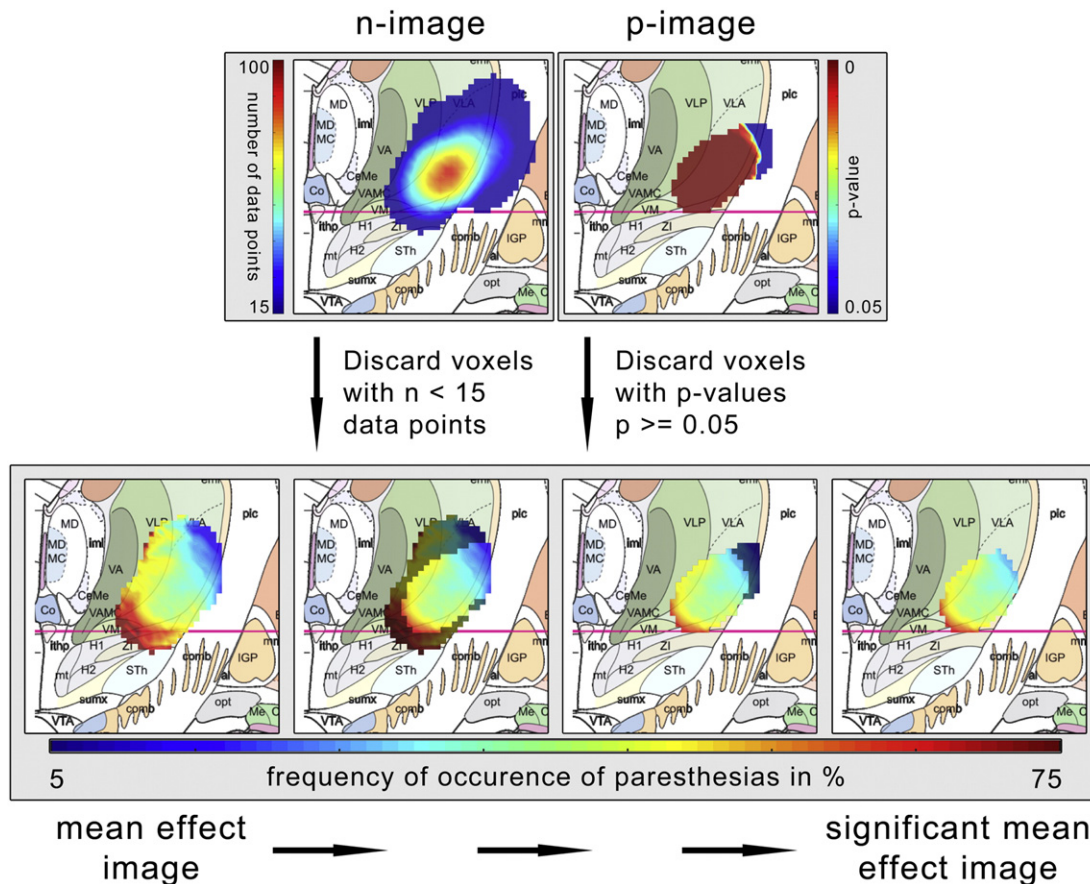


Fig. 2. Process of creating the 'significant mean effect image'. Process description of creating the 'significant mean effect image'. From left to right: First all VNAs are assigned their clinical values (in this example occurrence of paresthesia) and pooled to create the 'mean effect image'. Then all voxels that are not part of at least 15 VNAs, as can be seen in blue in the n-image, are discarded (greyed out below). Next, voxel-wise statistical analysis is performed and all voxels with p-values ≥ 0.05 , as can be seen in blue in the p-image, are rejected (greyed out below). The remaining voxels compose the 'significant mean effect image'. Data is displayed at 14.6 mm posterior to the anterior commissure and onto the respective atlas slice (Mai et al., 2008). Color coding can be inferred from the respective colorbars.

significance of our PSMs, we first created a summary statistic Q by summing up the negative decadic logarithms of each significant p -value in the p -image:

$$Q = \sum_i \{-\log p_i \mid p_i \leq .05\} \quad (2)$$

(see Eisenstein et al., 2014.)

We then created permutations of the original dataset by randomly reassigning the relationship between the measured clinical outcomes and the VNAs. Because stimulation amplitude was correlated to certain clinical outcomes, our permutation algorithm was restricted to maintain the relationship between clinical values and stimulation amplitude. This means that to each VNA a random clinical value of the original dataset was reassigned, as long as this clinical value was originally assigned to a VNA with the same stimulation amplitude. After thus creating a new, permuted dataset, a new 'p-image' and new summary statistic were calculated. These steps were repeated one thousand times, which resulted in one thousand summary statistics. To decide upon the overall significance of the original PSM, the original summary statistic Q was compared to the permuted ones. Q was deemed significant if it was >95% of the other summary statistics or, in other words, ranked higher than 950 of the 1000 summary statistics. In this case the original PSM was accepted as valid.

2.8. Further analysis

If a PSM was deemed valid, we further analyzed its relation to the surrounding neuroanatomy. We focused on the VIM, the ZI and the neighboring parts of the thalamus, namely the ventral posterolateral (VPL), the ventral posteromedial (VPM), the ventral posterior inferior (VPI), the centromedian (CM), the ventral lateral anterior (VLA) and

the ventral anterior (VA) nuclei. For each valid PSM, we calculated what percentage of the PSM covered the respective neuroanatomical structure (Table 2) and how much of the structure was covered by the PSM (Table 1). We also calculated non-weighted means over the mean effect scores of the PSM's voxels for each structure they lay in separately, to determine how strong the average stimulation effect was, when stimulating inside that structure. To determine the 'hotspot' of each PSM we repeated this on Volumes which incorporated only the 10% of the PSM's voxels which had the highest values of tremor suppression or side-effect elicitation (Table 3). To compare postural tremor suppression in the VIM to tremor suppression in the ZI we statistically compared the PSM's voxels inside the two structures using a Wilcoxon rank-sum test.

2.9. Technical realization

All computational work was carried out with MATLAB 2015b (The MathWorks Inc., Natick, Massachusetts, United States) on a DELL Precision T7600 Workstation with two Intel Xeon E5-2665 CPUs and 64 GB RAM (Dell Inc., Round Rock, Texas, United States).

3. Results

3.1. Probabilistic stimulation maps

Significant mean effect images were created for tremor suppression (Fig. 3) and side-effects (Fig. 4). Nonparametric permutation testing confirmed overall validity for postural tremor suppression (Rank 1000/1000), paresthesia (Rank 1000/1000), dizziness (Rank 1000/1000), and dysarthria (Rank 998/1000). Intention tremor suppression (Rank 336/1000) and disturbed vision (Rank 733/1000) did not reach

Table 1
Neuroanatomical structures covered by valid PSMs.

		Postural tremor	Paresthesia	Dysarthria	Dizziness
VIM	No. of voxels covered	3473 of 8670	3163 of 8670	955 of 8670	999 of 8670
	Percentage covered	40.06 %	36.48 %	11.01 %	11.52 %
ZI	No. of voxels covered	788 of 2276	819 of 2276	51 of 2276	604 of 2276
	Percentage covered	34.62 %	35.98 %	2.24 %	26.54 %
VPM	No. of voxels covered	617 of 965	627 of 965	161 of 965	590 of 965
	Percentage covered	63.94 %	64.97 %	16.68 %	61.14 %
VPI	No. of voxels covered	303 of 622	309 of 622	0 of 622	250 of 622
	Percentage covered	48.71 %	49.68 %	0.00 %	40.19 %
VPL	No. of voxels covered	1124 of 5054	1149 of 5054	185 of 5054	511 of 5054
	Percentage covered	22.24 %	22.73 %	3.66 %	10.11 %
CM	No. of voxels covered	918 of 2375	968 of 2375	119 of 2375	533 of 2375
	Percentage covered	38.65 %	40.76 %	5.01 %	22.44 %
VA	No. of voxels covered	42 of 4159	47 of 4159	7 of 4159	0 of 4159
	Percentage covered	1.01 %	1.13 %	0.17 %	0.00 %
VLA	No. of voxels covered	1543 of 3763	1379 of 3763	800 of 3763	215 of 3763
	Percentage covered	41.00 %	36.65 %	21.26 %	5.71 %

Legend: The number of voxels of a certain neuroanatomical structure, that were covered by a PSM are listed as well as the percentage with respect to the total number of voxels that were assigned to the structure in the atlas. Highest values for each PSM are highlighted in dark gray/light gray.

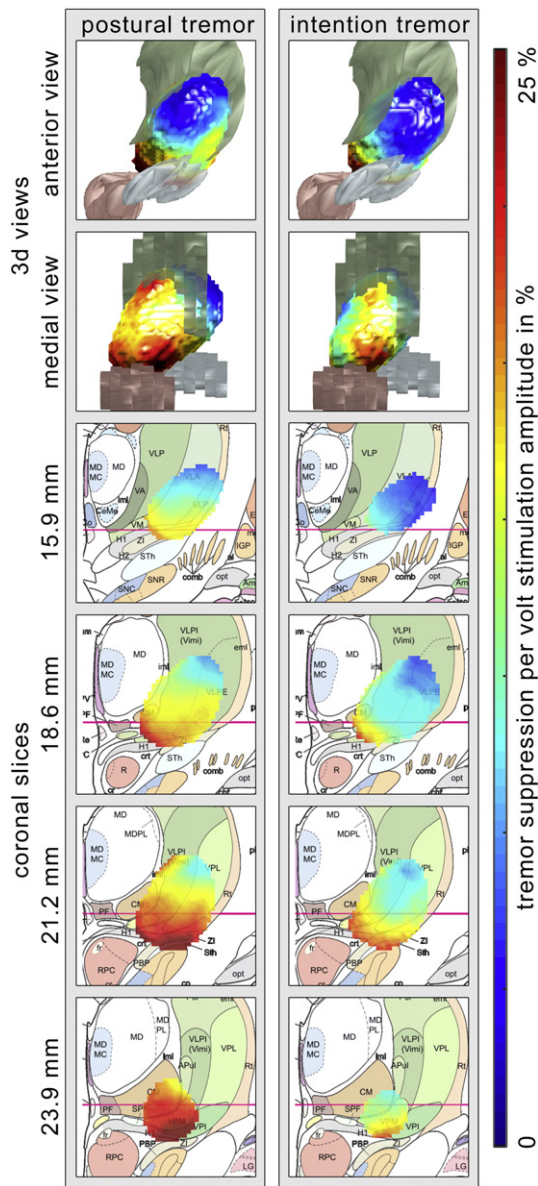


Fig. 3. PSMs for tremor suppression. Significant mean effect images for the suppression of postural tremor (left column) and intention tremor (right column). In the top two rows, 3d volumes, encompassing all voxels with a statistically significant tremor reduction, are shown together with the VIM (green), the subthalamic nucleus (blue), and the red nucleus (red). Below, coronal slices through these volumes are plotted onto the respective atlas slice (distances in mm posterior to the anterior commissure) (Mai et al., 2008). Color coding of the significant mean effect image (volumes and slices) indicates the mean tremor per volt of stimulation amplitude, with blue indicating lower and red indicating higher tremor suppression. Exact values can be inferred from the colorbar. Note that PSM for intention tremor suppression did not reach overall significance during the validation process.

validity. Valid PSMs covered several neuroanatomical structures (Table 1). Overlaps between the valid PSMs and multiple neuroanatomical structures and the respective, structure-specific scores were calculated and are summarized in Table 2. These steps were also repeated for each PSM's hotspot which incorporated only the 10% of voxels with the highest scores (Table 3).

3.2. Tremor

While in the voxel-wise statistical analysis both intention tremor and postural tremor were reduced by stimulation in a large area, only the PSM for postural tremor could be statistically validated. Upon visual

inspection stimulation was most effective in the most ventral parts of the thalamus and in the ZI. Hotspot analysis confirmed this impression with 37% of the best 10% of voxels lying inside the ZI and only 2% lying inside the VIM. Mean postural tremor suppression of significant voxels inside the ZI was significantly higher than inside the VIM (ZI = 20.71%/V, VIM = 13.47%/V, $p < 0.001$).

3.3. Side-effects

Paresthesia was most likely caused by stimulation ventral and posterior of the VIM in the ZI, the VPM and the VPL. The highest probability of eliciting dizziness was observed for voxels slightly more anterior in the ZI, the VPM and the PM. Dysarthria showed overall significance in the nonparametric permutation testing and hotspot analysis showed most of the voxels to lie inside the VLA. However upon visual inspection the ragged spatial distribution of the PSM for dysarthria did not allow drawing further conclusions about the neuroanatomical origin of the effects.

4. Discussion

4.1. Tremor suppression

Our results provide further indications that the ZI/PSA constitutes an effective and possibly more efficient DBS target than the VIM proper for suppressing limb tremor (Barbe et al., 2011; Blomstedt et al., 2010; Herzog et al., 2007; Sandvik et al., 2012; Xie et al., 2012). While the PSMs for intention and postural tremor look quite similar regarding their spatial distribution, overall tremor suppression scores were lower for intention tremor. At first sight it may seem counterintuitive that the PSM for intention tremor suppression did not reach overall significance despite its distinct, spatial distribution, which is very unlikely to be purely coincidental. Note, however, that only the sum of all significant p-values and no spatial information was used to generate the summary statistic and determine overall significance. This might explain why permuted datasets, which in general show a far more even spatial distribution, could have ranked higher than the original dataset.

4.2. Side-effects

Paresthesia occurred mainly due to DBS in the ventral posterior thalamus (VPM VPI) and the ZI, which is also in line with previously published results (Fytogoridis et al., 2013; Kuncel et al., 2008). The ventral posterior thalamus is known to receive sensory input from the medial lemniscus (VPL) and the trigeminal pathway (VPM) (Purves and Williams, 2001). Unfortunately our clinical data did not include information whether paresthesias occurred temporarily or persisted, which is important with regard to long-term stimulation outcome. The PSM for dizziness showed a ventro-medial hotspot, which might be linked to fibers of the vestibular system running medial to the medial lemniscus and targeting the more posteromedial parts of the thalamus (Dieterich et al., 2005; Zwergal et al., 2008). PSMs for dysarthria and disturbed vision showed no clear spatial distribution which might be due to the relatively small number of patients who experienced these side-effects.

4.3. Atlas and anatomical accuracy

The 'atlas-approach' used in this study might be considered a limitation since using a neuroanatomical atlas as the frame of reference neglects individual anatomical variability. However, standardization of neuroanatomical data is needed when analyzing multiple subjects. Importantly, the method of rigid atlas registration used in this study has been shown to have high accuracy of below 1 mm for subthalamic structures (Videen et al., 2008), which is in the range of the accuracy that can be achieved in neuroimaging. Also while using individual imaging data might be more accurate in analyzing the neuroanatomical

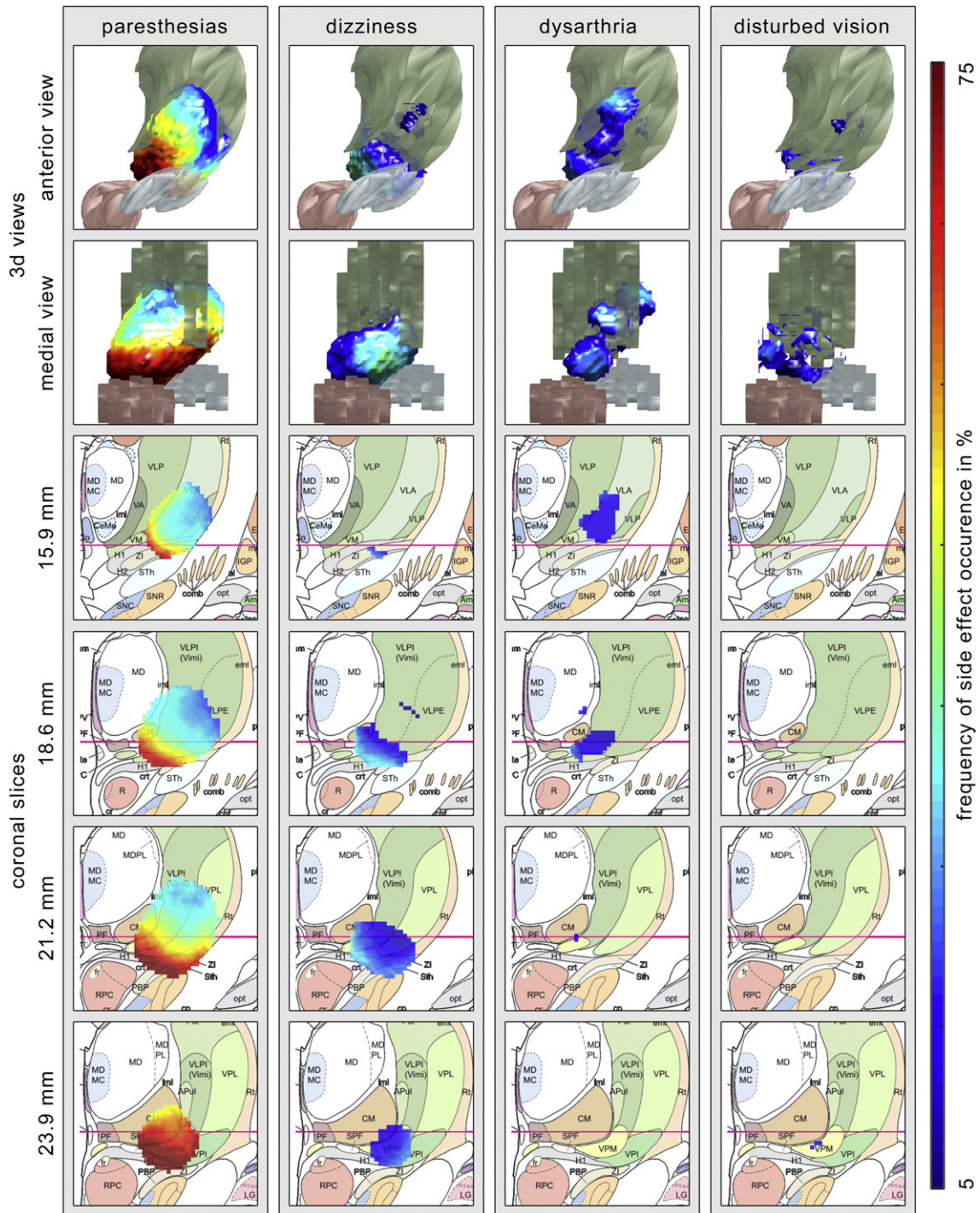


Fig. 4. PSMs for side-effects. Significant mean effect images for eliciting stimulation-induced side-effects. Side-effects shown from left to right are paresthesia, dizziness, dysarthria, and disturbed vision. In the top two rows, 3d volumes, encompassing all voxels which significantly elicited certain side-effects, are shown together with the VIM (green), the subthalamic nucleus (blue), and the red nucleus (red). Below, coronal slices through these volumes are plotted onto the respective atlas slice (distances in mm posterior to the anterior commissure) (Mai et al., 2008). Color coding of the significant mean effect image (volumes and slices) indicates the probability of eliciting a side effect, with blue indicating lower probability and red indicating higher probability. Exact values can be inferred from the colorbar. Note that the PSM for disturbed vision did not reach overall significance during the validation process.

origin of DBS effects in an individual patient, one has to keep in mind that there are several limitations to that kind of approach as well. These include technical problems like image resolution and/or distortion as well as inaccuracies in image registration or the problem of identifying neuroanatomical structures in MRI imaging. Despite its limitations, we are convinced that the ‘atlas-approach’ as employed here provides valuable probabilistic information due to the large number of data points included. While patients may differ in their individual

anatomy, there is no reason to assume that this introduces systematic deviations in a cohort of subjects. Another important point is that we pooled left- and right-hemispheric electrodes. While this increase in data of course improves the overall robustness of our PSMs, this approach will lose sensitivity to hemisphere-specific effects. For tremor suppression or paresthesia hemisphere-specific effects are unlikely. But side-effects like dysarthria might have a hemisphere-specific component. Given a symptom like dysarthria was primarily related to

Table 2
Structure-specific symptom suppression and side-effects for valid PSMs.

		Postural tremor	Paresthesia	Dysarthria	Dizziness
VIM	Percentage of PSM	38.31 %	36.46 %	43.27 %	27.03 %
	Mean score	13.47 %	34.13 %	11.08 %	11.15 %
ZI	Percentage of PSM	8.69 %	9.44 %	2.31 %	16.34 %
	Mean score	20.71 %	62.12 %	11.75 %	19.41 %
VPM	Percentage of PSM	6.81 %	7.23 %	7.29 %	15.96 %
	Mean score	21.65 %	68.35 %	13.45 %	17.73 %
VPI	Percentage of PSM	3.34 %	3.56 %	0.00 %	6.76 %
	Mean score	22.91 %	67.80 %	–	17.72 %
VPL	Percentage of PSM	12.40 %	13.24 %	8.38 %	13.83 %
	Mean score	16.28 %	36.87 %	7.60 %	11.33 %
CM	Percentage of PSM	10.13 %	11.16 %	5.39 %	14.42 %
	Mean score	18.84 %	55.19 %	13.20 %	16.69 %
VA	Percentage of PSM	0.46 %	0.54 %	0.32 %	0.00 %
	Mean score	5.58 %	47.95 %	21.15 %	–
VLA	Percentage of PSM	17.02 %	15.90 %	36.25 %	5.82 %
	Mean score	8.56 %	33.40 %	13.57 %	7.80 %

Legend: The percentage of voxels of validated PSMs which lay in the respective neuroanatomical structure, as well as the mean clinical score of the voxels in each structure are listed. Mean scores are shown in percentage of tremor reduction per stimulation volt for postural tremor and frequency of occurrence for the examined side-effects. Highest values for percentage and mean score are highlighted in dark gray/light gray.

stimulation of for example the left hemisphere, as has been suggested for DBS of the subthalamic nucleus (Schulz et al., 2012; Wang et al., 2006), pooling electrodes could lead to an underrepresentation of dysarthria in our PSMs. In the future, especially with larger datasets, it might be interesting to analyze hemispheres separately to investigate such effects.

4.4. VNA-model

As shown in the appendix our VNA-model allows for a simple radius estimate, which is in line with previously published studies (Astrom et al., 2015; Kuncel et al., 2008). A spherical VNA is of course a simplification and it has been shown that varying tissue properties like conductivity or fiber orientation might lead to complex changes in the spatial distribution of neural activation (Åström et al., 2011; Wårdell et al., 2014). While this can be highly relevant when analyzing neural activation in an individual subject with individual neuroimaging, we suggest that it is of less importance for the multi-subject atlas-approach used here. A possible in-between solution for multi-subject studies has been proposed by Butson et al., 2011, where instead of using individual diffusion tensor imaging (DTI) data they used a DTI-based atlas to modify their VNAs according to different tissue properties (Butson et al., 2011). In our opinion there are two principal ways of addressing the accuracy of VNA estimates: First, to use more complex individualized VNA-estimates, which might increase accuracy, but at the same time could increase the risk of ‘overfitting’ due to the complexity of the model and the many unknown details of the mechanisms of DBS. Second, to use simpler models and achieve accuracy through using larger datasets, which is the approach chosen for our current study. Another limitation is the assumption of electrode impedances of 1000 Ohms, although this assumption has been deemed reasonable in other publications as well (Gross and Rolston, 2008; Kuncel et al., 2008). Since voltage-controlled stimulation was used and since impedances are voltage-dependent, exact impedance recordings would be needed for every

single DBS-setting for increased data quality. Others have shown that impedance changes of 500 Ohms lead to a change in VNA radius of about 15% (Chaturvedi et al., 2013). Consecutively, impedance fluctuations in the usual range are expected to lead to changes in stimulation spread only in the submillimeter range. For future studies it remains to be seen how current-controlled devices might impact on the problem of varying impedances.

4.5. Statistics

The voxel-based statistical analysis used in this study was originally proposed by Eisenstein et al., 2014. To date it was the first and only approach that specifically deals with the statistical analysis of PSMs. While we adapted the general method we made several changes at different steps of the analysis. First and foremost, the original method did not include any VNA-model and thus did not account for different stimulation parameters, which varied highly in their cohort. Instead, it was based on electrode locations and a Gaussian weighting function that weighted clinical effects in a voxel only by the distance of that voxel from the stimulated electrode. As others discussed, this approach has the tendency to overemphasize on electrode location (Pallavaram et al., 2008) and might alter the real spatial distribution in these PSMs. Our data suggest that incorporating a VNA-model and thus taking stimulation settings into account provides relevant additional information that may improve the PSM’s accuracy. For our analysis we increased the number of clinical values needed to include a voxel in the statistical analysis from $n = 6$ to $n = 15$ to ensure validity of the voxel-wise statistics. We also used Wilcoxon signed-rank or binomial tests instead of t -tests because they better fitted the clinical data. Finally, we used one thousand cycles for our permutation algorithm instead of the two hundred cycles used by Eisenstein et al. This is in line with other publications that proposed a minimum of one thousand permutation cycles when analyzing larger datasets (Nichols and Holmes, 2002). The main disadvantage of this method is that overall statistical validation only confirms the p-image

Table 3
Structure-specific symptom suppression and side-effects for hotspots of valid PSMs.

		Postural tremor	Paresthesia	Dysarthria	Dizziness
VIM	Percentage of hotspot	1.77 %	0.00 %	24.29 %	5.85 %
	Mean score	23.66 %	–	24.39 %	28.42 %
ZI	Percentage of hotspot	37.20 %	23.90 %	0.95 %	22.84 %
	Mean score	25.02 %	82.38 %	23.03 %	29.76 %
VPM	Percentage of hotspot	21.52 %	27.37 %	10.48 %	16.43 %
	Mean score	23.96 %	80.68 %	23.49 %	30.00 %
VPI	Percentage of hotspot	18.76 %	13.63 %	0.00 %	2.23 %
	Mean score	24.57 %	80.00 %	–	26.94 %
VPL	Percentage of hotspot	1.55 %	0.58 %	0.00 %	1.67 %
	Mean score	23.22 %	82.36 %	–	26.64 %
CM	Percentage of hotspot	0.99 %	10.97 %	3.81 %	13.09 %
	Mean score	22.92 %	77.97 %	22.32 %	32.47 %
VA	Percentage of hotspot	0.00 %	0.00 %	1.43 %	0.00 %
	Mean score	–	–	25.39 %	–
VLA	Percentage of hotspot	0.00 %	0.00 %	40.48 %	0.28 %
	Mean score	–	–	25.12 %	27.78 %

Legend: The percentage of voxels of the hotspot which lay in the respective neuroanatomical structure, as well as the mean clinical score of the voxels in each structure are listed. Mean scores are shown in percentage of tremor reduction per stimulation volt for postural tremor and frequency of occurrence for the examined side-effects. Highest values for percentage and mean score are highlighted in dark gray/light gray.

as a whole – thereby ignoring the spatial distribution inside the PSM. Future approaches, based for example on the cluster size of significant voxels, may further improve this method.

4.6. Clinical data

We used a retrospective dataset of 16 ET-patients. Quality of the clinical data was limited due to the fact that there was only one clinician performing the clinical assessments who was not blinded regarding to stimulation parameters. Due to the retrospective nature of this study, the clinician was, however, unaware of the intention of this study while acquiring the clinical ratings. Therefore, we have no reason to assume that the lack of blinding might have confounded our data. The size of the patient collective is comparable to what has been used in other studies (Astrom et al., 2010; Butson et al., 2011; Frankemolle et al., 2010). However, our clinical data had the important advantage, that it included a multitude of stimulation conditions for each patient. While other studies often only examined one stimulation conditions, i.e. the clinical stimulation setting (Eisenstein et al., 2014), we analyzed up to 48 stimulation conditions in each patient resulting in over 600 different stimulation conditions in total. One disadvantage of using monopolar reviews is the short duration of about one to two minutes only in which each condition is examined. While this suffices for tremor

response and most side-effects (O'Suilleabhain et al., 2003), other potential effects might be overlooked.

4.7. Spatial distribution of PSMs

One of the biggest problems with probabilistic mapping of DBS effects is the limited spatial distribution of leads and consecutively the limited space covered by stimulation. Since neurosurgeons try to position the lead as accurately as possible in their respective target, a lot of data points exist for that target but little to no datapoints for the surrounding area. Probabilistic maps thus tend to overestimate the effects of the targeted area and underestimate the effects in the undersampled surroundings. The PSMs hotspot thus has the tendency to be quite similar to the mean location of examined electrodes, especially when only taking the best clinical stimulation settings into account (Cheung et al., 2014; Eisenstein et al., 2014). One way to at least partially avoid the problem of lacking electrode distribution is to use data from all implanted electrodes, not only the ones with best clinical outcome. Additionally, the PSMs can be refined by including suboptimal stimulation settings. Since suboptimal symptom suppression often occurs at low amplitudes, which impact voxels close to the stimulated electrode, including these settings can counterbalance the PSMs tendency to emphasize too much on its center area. For the future it will be important, to combine data from patients implanted by different surgeons at different

centers, since many surgeons use slightly different techniques for targeting. For certain effects, especially for side-effects, it might also be reasonable to pool data from different, but closely related DBS targets like for example the VIM, the PSA, and the STN to cover a larger area of the brain during PSM generation.

5. Conclusion

We here present a revised method for probabilistic mapping of DBS effects and demonstrate its use in ET-patients. It is the first study providing statistically validated and VNA-based PSMs for the thalamic region as well as for ET-patients. Within the examined target area our PSMs show stimulation of the ZI to be very effective in suppressing tremor. However we could also demonstrate that side-effects such as paresthesia and dizziness are most likely elicited inside or in close proximity to the ZI. Thus double-blinded clinical studies with long-term follow-up which compare ZI-DBS to VIM-DBS are warranted. The methods described here, can be used for other DBS targets or indications as well. Monopolar reviews, which are part of routine care in many DBS centers (Volkman et al., 2002), can be of particular use for probabilistic mapping to quickly generate large sets of clinical data. With more complex DBS systems being announced for the years to come, parameter selection will become increasingly difficult due to the vast amount of possible combinations. Already there have been approaches for software-assisted programming of DBS devices (Pourfar et al., 2015). PSMs can assist clinicians by providing population-based a priori information about expected DBS effects (Phibbs et al., 2014).

Acknowledgements

This study was supported by grants from the European Union (FP-7 IMPACT) and the German Research Foundation (KFO-219). MA is a full time employee at Medtronic Eindhoven Design Center. MTB received an unrestricted research grant from Medtronic (ODIS trial). VVV and LT reported financial and other support by Medtronic (EARLYSTIM trial), Boston Scientific (VANTAGE and REGISTRY trial), St. Jude Medical and Sapiens steering brain stimulation (FP- 7 IMPACT). We thank Fabienne Jung, Nadine Apetz, Paul Reker and Immo Weber of the Cologne movement disorders research group for providing help and criticism.

Appendix A. Supplementary data

Supplementary data to this article can be found online at <http://dx.doi.org/10.1016/j.nicl.2016.11.019>.

References

Astrom, M., Tripoliti, E., Hariz, M.J., Zrinzo, L.U., Martinez-Torres, I., Limousin, P., Wardell, K., 2010. Patient-specific model-based investigation of speech intelligibility and movement during deep brain stimulation. *Stereotact. Funct. Neurosurg.* 88: 224–233. <http://dx.doi.org/10.1159/000314357>.

Åström, M., Lemaire, J.-J., Wårdell, K., 2011. Influence of heterogeneous and anisotropic tissue conductivity on electric field distribution in deep brain stimulation. *Med. Biol. Eng. Comput.* 50:23–32. <http://dx.doi.org/10.1007/s11517-011-0842-z>.

Astrom, M., Diczfalusy, E., Martens, H., Wardell, K., 2015. Relationship between neural activation and electric field distribution during deep brain stimulation. *IEEE Trans. Biomed. Eng.* 62:664–672. <http://dx.doi.org/10.1109/TBME.2014.2363494>.

Barbe, M.T., Liebhart, L., Runge, M., Deyng, J., Florin, E., Wojtecki, L., Schnitzler, A., Allert, N., Sturm, V., Fink, G.R., Maarouf, M., Timmermann, L., 2011. Deep brain stimulation of the ventral intermediate nucleus in patients with essential tremor: stimulation below intercommissural line is more efficient but equally effective as stimulation above. *Exp. Neurol.* 230:131–137. <http://dx.doi.org/10.1016/j.expneurol.2011.04.005>.

Barbe, M.T., Pochmann, J., Lewis, C.J., Allert, N., Wirths, J., Visser-Vandewalle, V., Timmermann, L., 2014. Utilization of predefined stimulation groups by essential tremor patients treated with VIM-DBS. *Parkinsonism Relat. Disord.* 20:1415–1418. <http://dx.doi.org/10.1016/j.parkreldis.2014.09.021>.

Blomstedt, P., Sandvik, U., Tisch, S., 2010. Deep brain stimulation in the posterior subthalamic area in the treatment of essential tremor. *Mov. Disord.* 25:1350–1356. <http://dx.doi.org/10.1002/mds.22758>.

Butson, C.R., Cooper, S.E., Henderson, J.M., Wolgamuth, B., McIntyre, C.C., 2011. Probabilistic analysis of activation volumes generated during deep brain stimulation. *NeuroImage* 54:2096–2104. <http://dx.doi.org/10.1016/j.neuroimage.2010.10.059>.

Chaturvedi, A., Luján, J.L., McIntyre, C.C., 2013. Artificial neural network based characterization of the volume of tissue activated during deep brain stimulation. *J. Neural Eng.* 10:56023. <http://dx.doi.org/10.1088/1741-2560/10/5/056023>.

Cheung, T., Noecker, A.M., Alterman, R.L., McIntyre, C.C., Tagliati, M., 2014. Defining a therapeutic target for pallidal deep brain stimulation for dystonia. *Ann. Neurol.* 76:22–30. <http://dx.doi.org/10.1002/ana.24187>.

Dieterich, M., Bartenstein, P., Spiegel, S., Bense, S., Schwaiger, M., Brandt, T., 2005. Thalamic infarctions cause side-specific suppression of vestibular cortex activations. *Brain* 128:2052–2067. <http://dx.doi.org/10.1093/brain/awh551>.

Eisenstein, S.A., Koller, J.M., Black, K.D., Campbell, M.C., Lugar, H.M., Ushe, M., Tabbal, S.D., Karimi, M., Hershey, T., Perlmutter, J.S., Black, K.J., 2014. Functional anatomy of subthalamic nucleus stimulation in Parkinson disease. *Ann. Neurol.* 76:279–295. <http://dx.doi.org/10.1002/ana.24204>.

Fasano, A., Herzog, J., Raethjen, J., Rose, F.E.M., Muthuraman, M., Volkman, J., Falk, D., Elble, R., Deuschl, G., 2010. Gait ataxia in essential tremor is differentially modulated by thalamic stimulation. *Brain* 133:3635–3648. <http://dx.doi.org/10.1093/brain/awq267>.

Flora, E.D., Perera, C.L., Cameron, A.L., Maddern, G.J., 2010. Deep brain stimulation for essential tremor: a systematic review. *Mov. Disord.* 25:1550–1559. <http://dx.doi.org/10.1002/mds.23195>.

Frankemolle, A.M.M., Wu, J., Noecker, A.M., Voelcker-Rehage, C., Ho, J.C., Vitek, J.L., McIntyre, C.C., Alberts, J.L., 2010. Reversing cognitive–motor impairments in Parkinson's disease patients using a computational modelling approach to deep brain stimulation programming. *Brain* 133:746–761. <http://dx.doi.org/10.1093/brain/awp315>.

Fytasgoridis, A., Åström, M., Wårdell, K., Blomstedt, P., 2013. Stimulation-induced side effects in the posterior subthalamic area: distribution, characteristics and visualization. *Clin. Neurol. Neurosurg.* 115:65–71. <http://dx.doi.org/10.1016/j.clineuro.2012.04.015>.

Gross, R.E., Rolston, J.D., 2008. The clinical utility of methods to determine spatial extent and volume of tissue activated by deep brain stimulation. *Clin. Neurophysiol.* 119: 1947–1950. <http://dx.doi.org/10.1016/j.clinph.2008.06.003>.

Herzog, J., Hamel, W., Wenzelburger, R., Pötter, M., Pinsker, M.O., Bartussek, J., Morsnowski, A., Steigerwald, F., Deuschl, G., Volkman, J., 2007. Kinematic analysis of thalamic versus subthalamic neurostimulation in postural and intention tremor. *Brain* 130:1608–1625. <http://dx.doi.org/10.1093/brain/awm077>.

Koller, W.C., Lyons, K.E., Wilkinson, S.B., Troster, A.I., Pahwa, R., 2001. Long-term safety and efficacy of unilateral deep brain stimulation of the thalamus in essential tremor. *Mov. Disord.* 16:464–468. <http://dx.doi.org/10.1002/mds.1089>.

Kuncel, A.M., Cooper, S.E., Grill, W.M., 2008. A method to estimate the spatial extent of activation in thalamic deep brain stimulation. *Clin. Neurophysiol.* 119:2148–2158. <http://dx.doi.org/10.1016/j.clinph.2008.02.025>.

Louis, E.D., Ferreira, J.J., 2010. How common is the most common adult movement disorder? Update on the worldwide prevalence of essential tremor. *Mov. Disord.* 25: 534–541. <http://dx.doi.org/10.1002/mds.22838>.

Mädler, B., Coenen, V.A., 2012. Explaining clinical effects of deep brain stimulation through simplified target-specific modeling of the volume of activated tissue. *Am. J. Neurosurg.* 115:1072–1080. <http://dx.doi.org/10.3174/ajnr.A2906>.

Mai, J.K., Paxinos, G., Voss, T., 2008. *Atlas of the Human Brain*. Academic Press, New York; London.

Maks, C.B., Butson, C.R., Walter, B.L., Vitek, J.L., McIntyre, C.C., 2009. Deep brain stimulation activation volumes and their association with neurophysiological mapping and therapeutic outcomes. *J. Neurol. Neurosurg. Psychiatry* 80:659–666. <http://dx.doi.org/10.1136/jnnp.2007.126219>.

McIntyre, C.C., Mori, S., Sherman, D.L., Thakor, N.V., Vitek, J.L., 2004. Electric field and stimulating influence generated by deep brain stimulation of the subthalamic nucleus. *Clin. Neurophysiol.* 115:589–595. <http://dx.doi.org/10.1016/j.clinph.2003.10.033>.

Mikos, A., Bowers, D., Noecker, A.M., McIntyre, C.C., Won, M., Chaturvedi, A., Foote, K.D., Okun, M.S., 2011. Patient-specific analysis of the relationship between the volume of tissue activated during DBS and verbal fluency. *NeuroImage* 54 (Supplement 1): S238–S246. <http://dx.doi.org/10.1016/j.neuroimage.2010.03.068>.

Mücke, D., Becker, J., Barbe, M.T., Meister, I., Liebhart, L., Roettger, T.B., Dembek, T., Timmermann, L., Grice, M., 2014. The effect of deep brain stimulation on the speech motor system. *J. Speech Lang. Hear. Res.* 57:1206–1218. <http://dx.doi.org/10.1044/2014.JSLHR-S-13-0155>.

Nichols, T.E., Holmes, A.P., 2002. Nonparametric permutation tests for functional neuroimaging: a primer with examples. *Hum. Brain Mapp.* 15:1–25. <http://dx.doi.org/10.1002/hbm.1058>.

O'Suilleabhain, P.E., Frawley, W., Giller, C., Dewey, R.B., 2003. Tremor response to polarity, voltage, pulsewidth and frequency of thalamic stimulation. *Neurology* 60, 786–790.

Pahwa, R., Lyons, K.E., Wilkinson, S.B., Simpson, R.K., Ondo, W.G., Tarsy, D., Norregaard, T., Hubble, J.P., Smith, D.A., Hauser, R.A., Jankovic, J., 2006. Long-term evaluation of deep brain stimulation of the thalamus. *J. Neurosurg.* 104:506–512. <http://dx.doi.org/10.3171/jns.2006.104.4.506>.

Pallavaram, S., D'Haese, P.-F., Kao, C., Yu, H., Rempel, M., Neimat, J., Konrad, P., Dawant, B., 2008. A new method for creating electrophysiological maps for DBS surgery and their application to surgical guidance. *Med. Image Comput. Comput.-Assist. Interv. MICCAI Int. Conf. Med. Image Comput. Comput.-Assist. Interv.* 11, pp. 670–677.

Phibbs, F.T., Pallavaram, S., Tolleson, C., D'Haese, P.-F., Dawant, B.M., 2014. Use of efficacy probability maps for the post-operative programming of deep brain stimulation in essential tremor. *Parkinsonism Relat. Disord.* 20:1341–1344. <http://dx.doi.org/10.1016/j.parkreldis.2014.09.004>.

Pourfar, M.H., Mogilner, A.Y., Farris, S., Giroux, M., Gillego, M., Zhao, Y., Blum, D., Bokil, H., Pierre, M.C., 2015. Model-based deep brain stimulation programming for Parkinson's disease: the GUIDE pilot study. *Stereotact. Funct. Neurosurg.* 93:231–239. <http://dx.doi.org/10.1159/000375172>.

- Chapter 9: the somatic sensory system. In: Purves, D., Williams, S.M. (Eds.), *Neuroscience*, second ed. Sinauer Associates, Sunderland, Mass.
- Sandvik, U., Koskinen, L.-O., Lundquist, A., Blomstedt, P., 2012. Thalamic and subthalamic deep brain stimulation for essential tremor: where is the optimal target? *Neurosurgery* 70:840–846. <http://dx.doi.org/10.1227/NEU.0b013e318236a809>.
- Schulz, G.M., Hosey, L.A., Bradberry, T.J., Stager, S.V., Lee, L.-C., Pawha, R., Lyons, K.E., Metman, L.V., Braun, A.R., 2012. Selective left, right and bilateral stimulation of subthalamic nuclei in Parkinson's disease: differential effects on motor, speech and language function. *J. Parkinsons Dis.* 2:29–40. <http://dx.doi.org/10.3233/JPD-2012-11049>.
- Siddon, R.L., Barth, N.H., 1987. Stereotaxic localization of intracranial targets. *Int. J. Radiat. Oncol. Biol. Phys.* 13:1241–1246. [http://dx.doi.org/10.1016/0360-3016\(87\)90201-X](http://dx.doi.org/10.1016/0360-3016(87)90201-X).
- Videen, T.O., Campbell, M.C., Tabbal, S.D., Karimi, M., Hershey, T., Perlmutter, J.S., 2008. Validation of a fiducial-based atlas localization method for deep brain stimulation contacts in the area of the subthalamic nucleus. *J. Neurosci. Methods* 168:275–281. <http://dx.doi.org/10.1016/j.jneumeth.2007.10.007>.
- Volkman, J., Herzog, J., Kopper, F., Deuschl, G., 2002. Introduction to the programming of deep brain stimulators. *Mov. Disord.* 17:S181–S187. <http://dx.doi.org/10.1002/mds.10162>.
- Wang, E.Q., Metman, L.V., Bakay, R.A.E., Arzbaecher, J., Bernard, B., Corcos, D.M., 2006. Hemisphere-specific effects of subthalamic nucleus deep brain stimulation on speaking rate and articulatory accuracy of syllable repetitions in Parkinson's disease. *J. Med. Speech-Lang. Pathol.* 14, 323–334.
- Wårdell, K., Kefalopoulou, Z., Diczfalusy, E., Andersson, M., Åström, M., Limousin, P., Zrinzo, L., Hariz, M., 2014. Deep brain stimulation of the pallidum internum for Gilles de la Tourette syndrome: a patient-specific model-based simulation study of the electric field. *NeuroModulation Technol. Neural Interface n/a-n/a*. [10.1111/ner.12248](https://doi.org/10.1111/ner.12248).
- Xie, T., Bernard, J., Warnke, P., 2012. Post subthalamic area deep brain stimulation for tremors: a mini-review. *Transl. Neurodegener.* 1:20. <http://dx.doi.org/10.1186/2047-9158-1-20>.
- Zhang, K., Bhatia, S., Oh, M.Y., Cohen, D., Angle, C., Whiting, D., 2010. Long-term results of thalamic deep brain stimulation for essential tremor: clinical article. *J. Neurosurg.* 112:1271–1276. <http://dx.doi.org/10.3171/2009.10.JNS09371>.
- Zwergal, A., Büttner-Ennever, J., Brandt, T., Strupp, M., 2008. An ipsilateral vestibulothalamic tract adjacent to the medial lemniscus in humans. *Brain* 131: 2928–2935. <http://dx.doi.org/10.1093/brain/awn201>.